doi:10.1016/j.jmb.2006.07.005 J. Mol. Biol. (2006) 362, 102–113

JMB

Available online at www.sciencedirect.com

ScienceDirect

ELSEVIER

Variable Dimerization of the Ly49A Natural Killer Cell Receptor Results in Differential Engagement of its MHC Class I Ligand

Julie Dam[1]†, James Baber[2]†, Alexander Grishaev[2]† Emilio L. Malchiodi[1], Peter Schuck[3], Ad Bax[2]* and Roy A. Mariuzza[1]*

[1]*Center for Advanced Research in Biotechnology, W. M. Keck Laboratory for Structural Biology, University of Maryland Biotechnology Institute, Rockville, MD 20850, USA*

[2]*Laboratory of Chemical Physics, National Institute of Diabetes and Digestive and Kidney Diseases, National Institutes of Health, Bethesda MD 20892, USA*

[3]*Division of Bioengineering and Physical Science, Office of Research Services, National Institutes of Health, Bethesda MD 20892, USA*

**Corresponding authors*

Natural killer (NK) cells play a vital role in the detection and elimination of virally infected and tumor cells. The Ly49 family of NK receptors regulates NK cell function by sensing major histocompatibility complex (MHC) class I molecules on target cells. Previous crystal studies revealed that the Ly49A homodimer binds one MHC molecule in an asymmetric interaction, whereas the Ly49C homodimer binds two MHC in a symmetrical fashion. Moreover, the bound receptors adopt distinctly different homodimeric forms: a "closed state" for Ly49A and an "open state" for Ly49C. Steric clashes between MHC molecules would preclude the closed Ly49A dimer from engaging two MHC in the manner of the open Ly49C dimer. To determine whether individual Ly49 receptors can undergo a conformational switch enabling them to bind MHC in different ways, we carried out a solution NMR study of unbound Ly49A, aided by dipolar coupling technology. This study reveals that, in solution, unligated Ly49A adopts a symmetric, open-state, homodimer conformation similar to that seen previously for Ly49C. Hence, Ly49A can assume both closed and open states. To address whether the Ly49A dimer can bind two MHC molecules in solution, besides the binding of one MHC observed in the crystal, we carried out analytical ultracentrifugation experiments. Velocity sedimentation demonstrates that the Ly49A dimer can engage two MHC molecules in solution, in agreement with NMR results showing that unbound Ly49A exists predominantly in the open state.

Keywords: NMR; NK cell receptor; Ly49A; MHC; residual dipolar coupling

Introduction

Natural killer (NK) cells are an essential component of innate immunity against virally infected and tumor cells.[1–3] The cytolytic activity of NK cells is regulated by a delicate balance of activating and inhibitory signals mediated through distinct classes of receptors found on their surface.[1,2] The dominant signal received by an NK cell through its interaction with normal levels of major histocompatibility complex (MHC) class I molecules on target cells is inhibitory. If the level of MHC class I is reduced through infectious or tumorigenic processes, this inhibitory signal is attenuated and the NK cell is activated.

Two distinct structural families of receptors are responsible for regulating NK cell function by monitoring expression of MHC or MHC-like molecules on surrounding cells: the C-type lectin-like NK receptors (Ly49s, NKG2D, CD94/NKG2) and the immunoglobulin-like NK receptors (KIRs, LIRs).[4] Ly49 receptors, of which there are at least 23 members (Ly49A–W), constitute the main MHC class I-monitoring receptor family on mouse NK

† J.D., J.B. and A.G. contributed equally to this work.

Present address: J. Dam, Institut Cochin, Département de Biologie Cellulaire, INSERM U 567, CNRS UMR 8104, 22 rue Mechain, 75014 Paris, France.

Abbreviations: NK, natural killer; NKD, natural killer receptor domain; MHC, major histocompatibility complex; NOE, nuclear Overhauser enhancement; RDC, residual dipolar coupling; TROSY, transverse relaxation optimized spectroscopy; SVD, singular value decomposition; PMF, potential of mean force.

E-mail addresses of the corresponding authors: bax@nih.gov; mariuzza@carb.nist.gov

0022-2836/$ - see front matter. Published by Elsevier Ltd.

cells.[2,5] Individual Ly49s recognize multiple, but not all, H-2D and H-2K MHC class I molecules. Ly49 receptors are homodimeric type II glycoproteins, with each chain composed of a C-type lectin-like domain, termed the natural killer receptor domain (NKD), connected by a stalk of approximately 70 residues to the transmembrane and cytoplasmic domains. Crystal structures have been determined for Ly49A bound to H-2D^d, Ly49C bound to H-2K^b, and Ly49I in the free form.[6–8]

In the Ly49A/H-2D^d complex (Figure 1(a)),[6] the Ly49A homodimer engages H-2D^d asymmetrically at a broad cavity underneath the peptide-binding platform of the MHC in a region that partially overlaps the CD8 binding site. Here, the Ly49A dimer makes contacts, through one of its subunits, with the α1/α2, α3 and β_2m domains of H-2D^d. In the crystal, the second Ly49A subunit was observed to contact a neighboring H-2D^d molecule at a different site, at one end of the peptide-binding platform (not shown).[6] However, subsequent mutagenesis studies of both Ly49A and H-2D^d identified unambiguously the region beneath the peptide-binding platform as the functional binding site for Ly49A on MHC that leads to inhibition of NK cell cytotoxicity.[9,10] By contrast, in the Ly49C/H-2K^b complex,[7] the Ly49C dimer engages H-2K^b bivalently, such that each subunit makes identical interactions with MHC class I at a site overlapping the Ly49A binding site on H-2D^d, to form a symmetrical, butterfly-shaped assembly (Figure 1(b)).

The structural basis for the very different modes of MHC engagement seen in the Ly49A/H-2D^d and Ly49C/H-2K^b complexes is the different dispositions of the Ly49A and Ly49C dimers. The Ly49A dimer adopts a "closed" conformation, such that NKD subunits are more closely juxtaposed than in the Ly49C dimer, which adopts an "open" conformation (Figure 1). Major steric clashes between MHC molecules would preclude the closed Ly49A dimer from binding two MHC simultaneously in the manner of the open Ly49C (or Ly49I) dimer. These findings from X-ray crystallography raise a number of important questions regarding MHC recognition by Ly49 receptors: Do the strikingly different modes of MHC class I engagement by Ly49A and Ly49C represent two "snapshots" of a single, coordinated assembly process followed by all Ly49 receptors in binding MHC, or do they correspond to two distinct solutions to MHC recognition adopted by different Ly49s? Do the open and closed forms of Ly49 receptors represent two basic alternatives for dimerization, existing in equilibrium, that every Ly49 can explore, or does each individual Ly49 adopt one or the other form, but not both?

To address whether individual Ly49 receptors can undergo a conformational switch that enables them to engage MHC in different ways, we determined the solution structure of the Ly49A homodimer, in unligated form, by NMR methods. In parallel, we used analytical ultracentrifugation to examine the binding of Ly49A to MHC class I in solution. The results obtained from our present NMR and ultracentrifuge measurements, in conjunction with those from earlier X-ray crystallography,[6–8] suggest a dynamic switch mechanism for Ly49 receptors in regulating NK cell cytolytic activity.

Results

Strategy for NMR study of Ly49A

At 30 kDa, the Ly49A dimer is only moderately large, but nevertheless it poses serious NMR challenges. In particular, the limited stability of the protein prevents the use of elevated temperatures, where solvent viscosity is lower and spectral appearance often is enhanced. Second, the substantial losses incurred during *in vitro* folding of the protein (see Materials and Methods), associated with the three disulfides per monomer, make generation of large quantities of the ^{2}H/^{13}C/^{15}N-

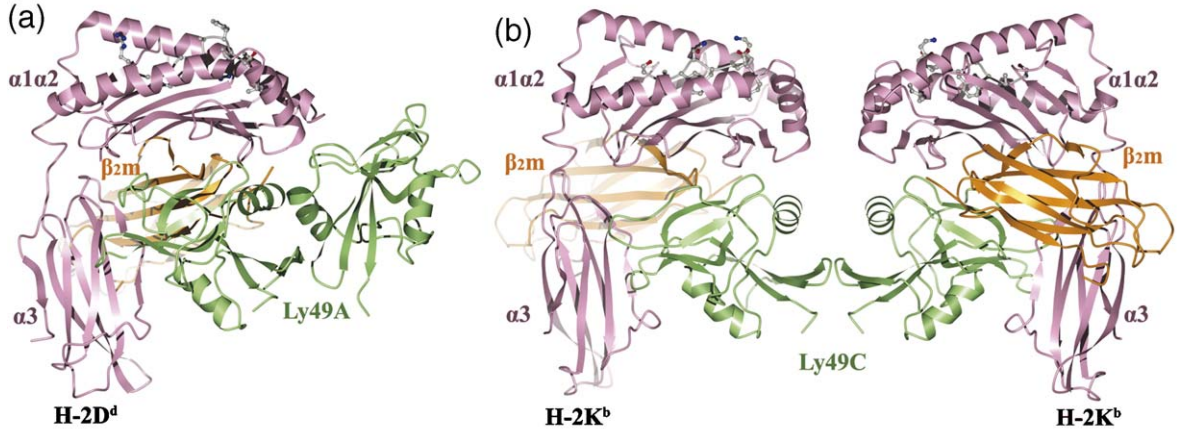

Figure 1. Structures of Ly49/MHC class I complexes. Domains are labeled. The α1, α2 and α3 domains of the MHC class I heavy chain are rose; β_2m is orange; the peptide in ball-and-stick representation is grey; the Ly49 molecules are green. (a) Ribbon diagram of Ly49A bound to H-2D^d (PDB accession code 1QO3). (b) Structure of Ly49C in complex with H-2K^b (1P4L).

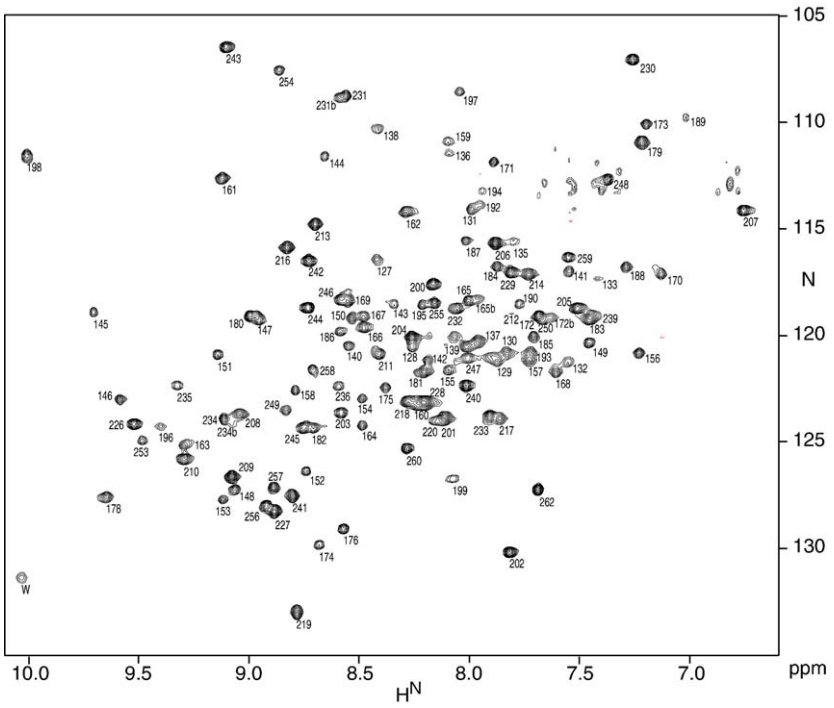

Figure 2. Two-dimensional 750-MHz ^{1}H-^{15}N TROSY-HSQC spectrum of U-^{2}H/^{15}N/^{13}C apo-Ly49A, in 95%/5% H_2O/$^{2}H_2O$. Correlations are labeled according to residue number, following the numbering scheme of PDB entry 1QO3.

enriched protein both labor-intensive and costly. Hence, it was important to follow an NMR strategy that minimizes sample requirements and measurement time, while nevertheless providing sufficient structural restraints to allow a detailed comparison of the solution structure to those solved previously by X-ray crystallography.

Conventionally, NMR structure determination has relied on the collection of a sufficiently large number of nuclear Overhauser enhancement (NOE) interactions, which, after conversion into semi-quantitative distance restraints, are used for deriving structures compatible with these restraints.[11] However, with the Ly49A monomer structure reasonably well established on the basis of prior crystal structures, the primary NOE information of interest focuses on the intermolecular NOEs. In principle, intermolecular interactions can be identified unambiguously by using a mixture of labeled and unlabeled protein, in combination with NMR isotope-filtering and editing procedures.[12,13] However, the sensitivity of such measurements is intrinsically fourfold lower compared to intramolecular interactions on the fully enriched protein, and therefore not easily applicable to Ly49A. Instead, we resort to the measurement of residual dipolar couplings (RDCs), which can be measured when the protein is dissolved in an aqueous medium containing a small volume fraction of magnetically oriented particles.[14,15] For the current study, we use the filamentous phage Pf1, which exhibits liquid crystalline alignment relative to an external magnetic field down to volume fractions well below 1%.[16,17] The presence of the oriented Pf1 particles in the Ly49A solution causes the distribution of protein orientations to deviate ever so slightly (about 0.1%) from being purely random, and permits the measurement of non-zero RDCs, which report on the time-averaged orientation of internuclear bond vectors relative to the magnetic field, and thereby relative to one another. First, this type of data then allows validation of the crystal structure of the Ly49A monomer as a model for its solution structure. Second, it tightly defines the relative orientation of the monomers in the homodimeric structure.

Measurement of one-bond RDCs does not provide translational information, and therefore does not define the intermolecular interface uniquely. The open and closed states of the Ly49A structures have, however, distinctly different intermolecular hydrogen bonding patterns. Pairing of β-strands in a fully perdeuterated protein, where the backbone amides have been back-exchanged to ^{1}H, can be determined readily from H^N-H^N NOEs in such a system, allowing the structure of Ly49A to be determined using only small quantities of protein and a moderate amount of measurement time.

Solution structure of apo-Ly49A

Our measurements focus on the globular extracellular domain of Ly49A, excluding the "stalk region" that connects the transmembrane domain with the Ly49A receptor domain (NKD). All previous attempts to crystallize Ly49A in unbound form (with or without the stalk) were unsuccessful, leading us to seek a structure determination by NMR. The present NMR study focuses on the NKD without the stalk, and in the absence of the MHC ligand. At 30 kDa and the relatively low temperature of 20 °C, ^{15}N transverse relaxation rates are quite high, making it necessary to rely on transverse relaxation optimized spectroscopy (TROSY) technology, combined with deuteration of all non-exchangeable protons, in order to reach sufficient

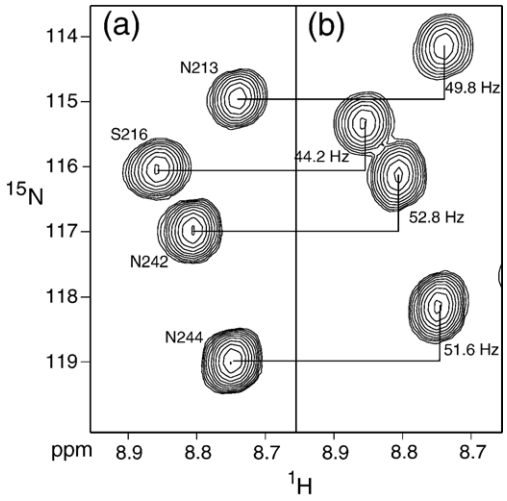

Figure 3. Small regions of projections on the ^{1}H-^{15}N plane of the 3D TROSY-HNCO (A) and 3D *J*-scaled ($\kappa = 1$) TROSY-HNCO spectra for the Pf1-aligned sample of apo-Ly49A. The difference in ^{15}N frequency for the correlations is marked and corresponds to $(^{1}J_{NH} + {}^{1}D_{NH})/2$.

spectral resolution and sensitivity.[18,19] The TROSY ^{1}H-^{15}N two-dimensional correlation map (Figure 2) displays a well-dispersed set of resonances, as expected for a protein rich in β-sheet. The spectrum exhibits a rather wide range of resonance intensities. Such intensity differences can arise from a number of sources: Particularly in perdeuterated proteins, the longitudinal relaxation time of buried amide protons can be quite long, exceeding 10 s, whereas the repetition rate of the experiment is typically optimized for more rapidly relaxing amides, found near the surface of the protein or in proximity to hydroxyl or other protons exchanging rapidly with the solvent. Although repeating the experiment with a much longer interscan delay of 10 s (data not shown) indicates that dispersion in longitudinal $^{1}H^{N}$ relaxation rates accounts for the low intensity of some of the resonances, it is not the only cause. There is also a doubling of resonances, mostly with a major and minor component (e.g., L234 at H^{N}, N = 9 ppm, 124 ppm), and a number of resonances that exhibit larger than average line width (e.g. A219 at N = 133 ppm). Although these weaker correlations typically did not yield sequential or intraresidue correlations between H^{N} and C^{β} in HN(CA)CB experiments, the combination of HNCA and HN(CO)CA together with the results of the 3D NOE experiments was sufficient to complete the sequential backbone assignment after regions with higher signal intensity had been uniquely assigned (see Supplementary Data for resonance assignments and representative data). Assignments were confirmed by use of the program MONTE.[20]

Measurement of RDCs was accomplished from both the difference in resonance frequency between TROSY and anti-TROSY ^{15}N components in a 3D HNCO-TROSY experiment, and from the difference in ^{15}N frequency between a 3D HNCO-TROSY and a *J*-scaled ($\kappa = 1$) HNCO-TROSY experiment.[21,22] Although the difference in ^{15}N resonance position in these latter two experiments (Figure 3) measures half the splitting, $(^{1}J_{NH} + {}^{1}D_{NH})/2$, the *J*-scaled HNCO-TROSY experiment yields higher resolution and more accurate peak positions than the anti-TROSY component in a regular HNCO-TROSY experiment, thereby compensating for the 50% smaller displacement. After doubling of the HSQC-derived RDC values, comparison with the results from the interleaved 3D HNCO-TROSY/anti-TROSY experiments showed good agreement (pairwise rmsd of 2.1 Hz), indicating a random uncertainty in their averaged values of slightly above 1 Hz. Singular value decomposition (SVD) fits[23] of the RDCs to the coordinates of a single Ly49A domain in the Ly49A/H-2D^{d} complex (PDB code *1QO3*)[6] shows a slightly better fit to the D-chain of Ly49A/H-2D^{d} (rmsd = 3.9 Hz; $Q = 38\%$; Figure 4(a)) than to its C-chain (rmsd = 4.5 Hz; $Q = 44\%$). The backbone rmsd between residues 140–258 of chains C and D of 1QO3 is 0.64 Å. As was noted previously,[6] even though the backbone

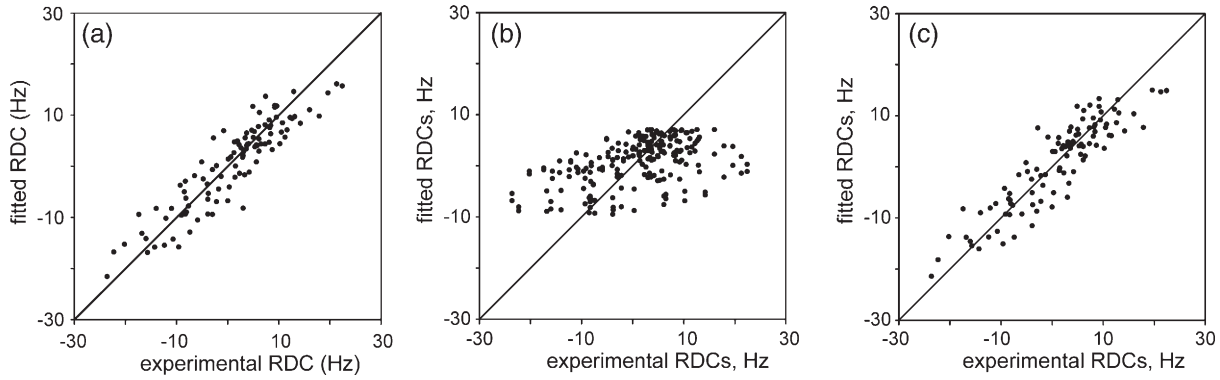

Figure 4. Correlation between experimental RDCs and values predicted by three different structural models. (a) Fit to the monomer (D-chain) of the Ly49A/H-2D^{d} X-ray structure. (b) Simultaneous fit of the RDCs to the dimeric Ly49A/H-2D^{d} X-ray structure, after the C-chain structure had been replaced by coordinates of the D-chain, best fitted to that of the C-chain. This procedure slightly improves the quality of the fit over a direct fit to the dimeric Ly49A/H-2D^{d} X-ray structure. (c) Fit to an "open" homodimeric Ly49A model where the D-chain of the Ly49A/H-2D^{d} X-ray structure is best fitted to the two Ly49C chains of the Ly49C/H-2K^{b} X-ray structure.

coordinates for the secondary structure elements of the two peptide chains in the asymmetric Ly49A/H-2D^d dimer superimpose quite well, the loop regions differ considerably in conformation. For a crystal structure determined at the moderate resolution of 2.3 Å, uncertainty in the atomic coordinates limits the accuracy at which RDCs can be predicted, and a *Q*-factor of 35% is typical for a structure solved at this level of resolution. If the SVD fit used to determine the alignment tensor is restricted to only the residues that are involved in secondary structure, a slightly better fit is obtained ($Q = 34\%$) but the turn and loop regions are less well predicted (44 vectors, $Q = 40\%$; Supplementary Data), even more so for chain C.

The fact that, with the exception of weak minor components for several residues not at the dimer interface, only a single set of resonances is observed for the homodimeric Ly49A domain indicates that, in solution, the dimer has C_2 symmetry. In order to evaluate whether the RDCs can distinguish between the open Ly49C-like form and the closed Ly49A dimer arrangement, we first generate symmetrized models for each of these two structures. For Ly49C this is accomplished by best fitting residues 140–258 of two copies of the D-chain of Ly49A to the corresponding residues of the Ly49C dimeric structure (PDB entry 1P4L). For Ly49A, the coordinates of the C-chain are replaced by those of the D-chain, when best-fitting the backbone atoms of the residues involved in secondary structure. When carrying out the SVD fit to the dimeric structure, any given RDC is fitted simultaneously to the orientations of the two corresponding N-H vectors in both halves of the dimer. In other words, the same measured value is assigned to the N-H vectors of a given residue in each of the two chains. A comparison of SVD fits between the experimental RDCs and the thus obtained structural models shows a much better fit to the open, Ly49C-like form of the protein than to the closed form (Figure 4(b) and (c)).

Rigid-body, molecular dynamics-based structure refinement of the dimer also strongly supports the open form conformation. In the absence of any distance restraint between the two chains, when using only RDCs, the relative orientation of the two monomers falls close to that observed in the open dimer conformation, such as the Ly49C 1P4L model, rather than the closed conformation observed in the Ly49A 1QO3 crystal structure.

The open Ly49C and closed Ly49A crystal structures (Figure 5), as observed in complexes with MHC,[6,7] exhibit distinctly different intermolecular H-bonds between the antiparallel β0 strands. Four and two backbone–backbone intermolecular H-bonds are found between the antiparallel β0 strands in the open and closed forms, respectively, with the register shifted by four residues between the two dimers (Figure 6).

In order to investigate whether the applicable H-bond configuration can be determined on the basis of RDCs alone, the two corresponding sets of H-bond restraints were generated and enforced by means of the recently described H-bond potential of mean force (PMF).[24] The PMF was activated for the following H-bonds: A 147O-B 145H^N; B 145O-A 147H^N; B 147O-A 145H^N; and A 145O-B 147H^N for the open form, and A 145O-B 143H^N and B 143O-A 145H^N for the closed form. When using the same rigid body refinement protocol, we find that the open form H-bond pairings are perfectly compatible with the domain orientations defined by the experimental RDCs. The resulting geometries of the interdomain H-bonds correspond to low PMF energies, indicating that these geometries are commonly found in the database of high-resolution X-ray structures that

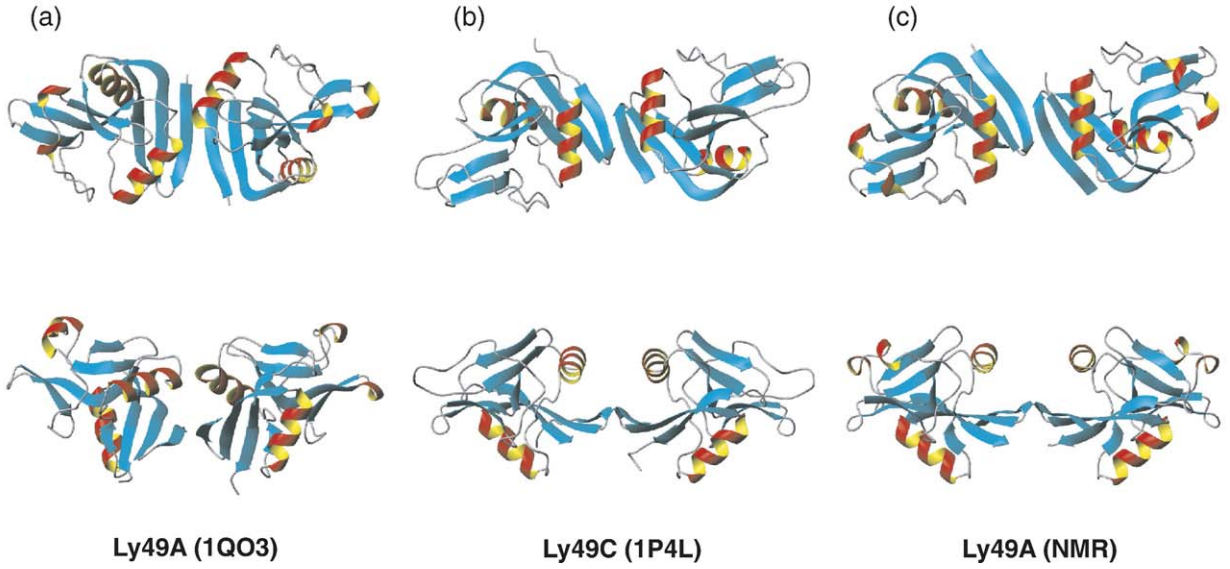

Figure 5. Variability in dimerization mode of Ly49 receptors. (a) Top and side views of the Ly49A homodimer (bound form), as observed in the Ly49A/H-2D^d X-ray structure.[6] (b) Top and side views of the Ly49C dimer (bound), as observed in the Ly49C/H-2K^b X-ray structure.[7] (c) Top and side views of Ly49A (unbound), as observed by solution NMR. In these ribbon models, the β-strands are cyan, the α-helices are red, and the loops are grey.

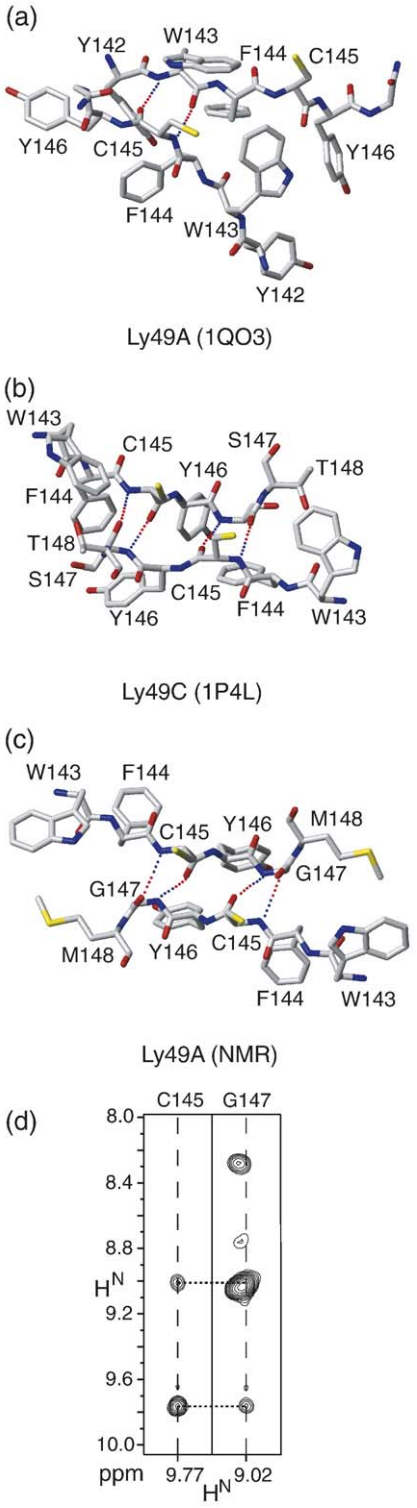

Figure 6. Hydrogen bonding pattern at the homodimeric interface. (a) Two asymmetric intermolecular H-bonds between W143-H^N–C145-CO and between W143-CO and C145-H^N are observed in the Ly49A/ H-$2D^d$ X-ray structure. (b) Two symmetric pairs of H-bonds between C145-H^N–G147-CO and between C145-CO and G147-H^N are observed in the open Ly49C X-ray structure, and (c) in the RDC-refined NMR structure of the apo-Ly49A homodimer. (d) Intermolecular NOE cross peaks between C145-H^N and G147-H^N. Note that the diagonal resonance of G147 at 9.02 ppm partially overlaps with that of E180.

underlies the PMF. At the same time, the quality of the RDC fit remains unchanged from that without the H-bond restraints (rmsd 3.9 Hz). In contrast, the two H-bond restraints observed in the closed conformation could not be satisfied simultaneously with the RDCs, with one of the two intermolecular H-bonds (W143O-C145H^N) broken and the O-H^N distance increased to ~2.9 Å, while the rmsd of the RDC fit increased to 4.1 Hz. Whereas this latter structure also yields several steric clashes between the two domains, as evaluated by the program MolProbity,[25] the RDC-refined structure with H-bond pairing based on the open conformation is free of high-energy steric interdomain contacts.

The different H-bond pairings for the Ly49A and Ly49C structures also predict distinctly different interdomain H^N-H^N NOEs (Figure 6(a) to (c)). Whereas the closed Ly49A structure predicts short interdomain H^N-H^N distances between V141 and G147 (3.4 Å) and between C145 and W143 (2.9 Å), neither of these interactions is observed in the 3D NOESY spectra. On the other hand, an intense NOE is observed between C145 and G147, which corresponds to a short (2.6 Å) distance in the open structure (Figure 6(d)), whereas the intradomain distance between C145-H^N and G147-H^N exceeds 6.7 Å. Therefore, the NOE data confirm the conclusion reached on the basis of the RDCs that in solution, in the absence of ligand H-$2D^d$, Ly49A predominantly adopts the open conformation and the interdomain base-pairing observed in the Ly49C and Ly49I structures.

Previous crystallographic data indicate that the alternative, closed conformation of Ly49A is also of low energy, at least in the presence of MHC ligand. A switch between the two conformations requires breaking of four (open→closed) or two (closed→open) intermolecular hydrogen bonds and a relatively major structural rearrangement. Such a process therefore is likely to take place on a timescale slower than microseconds. The absence of conformational exchange broadening at the interface in transverse relaxation measurements, and the absence of increased ^{15}N TROSY line-widths for amides at the dimer interface, indicates that the lifetime of the open state must be greater than ~100 ms. The absence of resonances that potentially could correspond to the closed form of the dimer in both the TROSY spectrum of Figure 1, even at levels as low as 2% relative to the signals of the symmetric dimer, and the absence of exchange peaks in the 3D ^1H-^{15}N-^1H NOESY spectrum (e.g. Figure 6(d)) put an upper limit of about 10% on the population of the closed form. If the population of the closed form were as high as 10%, its lifetime would be nine times shorter than that for the open form, i.e. longer than ca ~11 ms, and detectable resonances would become observable in the 2D and 3D spectra.

Ly49A binds two MHC molecules in solution

The finding by NMR that unbound Ly49A adopts a predominantly open conformation prompted us to

examine whether the Ly49A dimer could engage two MHC class I molecules in solution, in contrast to the crystal structure, where the closed Ly49A dimer binds only one MHC molecule (Figure 1(a)). Accordingly, we carried out sedimentation velocity analytical ultracentrifugation with the individual proteins and with mixtures (Figure 7). Sedimentation profiles were analyzed by the $c(s)$ size distribution method implemented in the software SEDFIT (see Materials and Methods).

At a concentration of 12 μM, Ly49A NKD behaved as a stable dimer, showing a single peak in the $c(s)$ profile with a sedimentation coefficient value of 2.75 S (Figure 7(a), continuous black line). Consistent with this result, Ly49A was found to dimerize with a dissociation constant (K_D) of approximately 500 nM, as measured by sedimentation equilibrium (data not shown). At 20 μM, H-2D^d is monomeric with an s value of 3.57 (Figure 7(a), broken black line). Analysis of mixtures by sedimentation velocity was carried out at different molar ratios, by mixing Ly49A (12 μM) with increasing concentrations of H-2D^d (7 M, 13 M, 20 M, 27 M, 40 M and 53 μM). The corresponding $c(s)$ distribution of the mixtures could be decomposed into several peaks (Figure 7(a)): a peak at 2.75 S corresponding to free Ly49A dimer, which disappears with increasing concentrations of MHC, a sharp peak at 3.57 S representing free H-2D^d, and broader peaks in the range of 3.7–5.6 S that clearly demonstrate an interaction between Ly49A and H-2D^d. The shift of peak position with increasing concentration of MHC and the broad shape of the complex peak suggest a relatively fast interaction between Ly49A and H-2D^d, with the peak positions reflecting the time-averaged association state of the reacting mixture, as predicted by Gilbert–Jenkins theory.[26] The range of complex peaks in the $c(s)$ distribution indicates the possibility of two different complexes with a 1:1 and 1:2 stoichiometry of Ly49A homodimer to H-2D^d. Integration of the $c(s)$ distribution gave weight-average s values as a function of H-2D^d concentration (Figure 7(b)), which were analyzed as described for the Ly49C/H-2K^b interaction.[7,27] Two different models were used, corresponding to one or two MHC-binding sites per Ly49A dimer. The analysis of weight-average s values was performed by fitting protein concentrations, K_Ds, and s values of the binding complexes. Alternatively, fitting was done by using a theoretical sedimentation coefficient of the complexes, obtained by hydrodynamic modeling, which is based on information from the Ly49C/H-2K^b and Ly49A/H-2D^d crystal structures (Figure 1).[28] Theoretical s values calculated for a complex in which one open Ly49C dimer binds one H-2K^b (1:1 complex) or two H-2K^b (1:2 complex) are 4.7 S and 6.3 S, respectively. For a 1:1 complex in which one closed Ly49A dimer binds one H-2D^d, the predicted s value is 5.0 S. Analysis of the weight-average sedimentation coefficient using a one-site model that closely fits the data led to a K_D of 116 μM, which is inconsistent with K_D measured by sedimentation equilibrium (10 μM), and to an s value for the 1:1

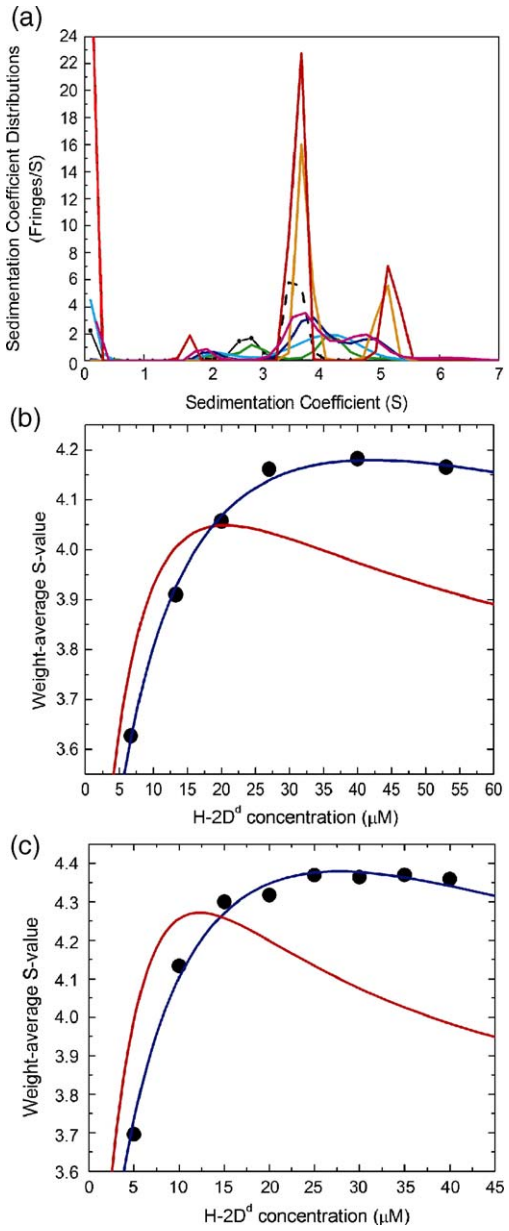

Figure 7. Sedimentation velocity analysis of the binding of Ly49A to H-2D^d. (a) Sedimentation coefficient distributions of wild-type Ly49A NKD alone (12 μM, continuous black line), of H-2D^d alone (20 μM, broken black line), and of mixtures. Ly49A (12 μM) was mixed with H-2D^d at 7 μM (green line), 13 μM (cyan line), 20 μM (blue line), 27 μM (violet line), 40 μM (orange line) and 53 μM (red line). (b) Dependence of the weight-average sedimentation coefficient on H-2D^d concentration for wild-type Ly49A. Each datum point corresponds to the integration of a c(s) distribution curve from (a). The lines show the best-fit weight-average S-value isotherms for a 1:1 Ly49A dimer/H-2D^d model (red line), and for a 1:2 Ly49A dimer/H-2D^d model (blue line). (c) Dependence of the weight-average sedimentation coefficient on H-2D^d concentration from sedimentation velocity experiments performed with the higher-affinity Ly49A Asp193Gly mutant. Each datum point corresponds to the integration of a c(s) distribution curve for a mixture of 9 μM Ly49A D193G with 5 μM, 10 μM, 15 μM, 20 μM, 25 μM, 30 μM, 35 μM, or 40 μM H-2D^d (data not shown). The lines show the best-fit weight-average S-value isotherms for a 1:1 model (red line) and a 1:2 model (blue line).

complex of 11 S, which even exceeds that predicted for a 1:2 complex (6.3 S). Likewise, analysis of weight-average s values using a one-site model, where the sedimentation coefficient of the 1:1 complex is implemented at its theoretical value (5.0 S), showed significant deviation from the experimental data (rms = 0.16) (Figure 7(b)). Conversely, a two-site model provided an excellent fit (rms = 0.012), with a K_D of 13 μM (similar to 10 μM determined by sedimentation equilibrium) and *s* values for the 1:1 and 1:2 complexes of 4.6 S and 6.2 S (close to the theoretical values of 4.7 S and 6.3 S).

As the affinity of Ly49A for H-2D^d is relatively weak (K_D = 10 μM), it was not possible to fully saturate the receptor with ligand, due to non-ideal sedimentation at the higher concentrations of H-2D^d needed to achieve saturation in this system. To achieve saturation, we increased the affinity of Ly49A for H-2D^d by mutating residue Gln193 of the NK receptor to Gly. We showed previously that this same mutation, identified by yeast display, increased the affinity of Ly49C for H-2K^b ~25-fold.[7] Although the Gln193Gly replacement improved binding of Ly49A to H-2D^d to a lesser degree (about fivefold, as measured by sedimentation equilibrium), this increase in affinity was sufficient to permit better saturation of the mutant Ly49A dimer. Thus, binding of Ly49A Gln193Gly to H-2D^d was analyzed as described above for the wild-type receptor. Whereas a one-site model could not describe the data well (rms = 0.254) (Figure 7(c)), a two-site model gave an excellent fit (rms = 0.024), with a K_D of 7 μM and *s* values for the 1:1 and 1:2 complexes of 4.6 S and 6.3 S, in good agreement with the theoretical values of 4.7 S and 6.3 S. Accordingly, for both wild-type and mutant Ly49A, analytical ultracentrifugation results demonstrating that the Ly49A dimer can engage two MHC molecules in solution are entirely compatible with the NMR structure of unbound Ly49A, where the dimer exists predominantly in the open conformation.

Discussion

We have shown by NMR that the Ly49A NK receptor adopts an open conformation in solution, different from the closed state observed previously by X-ray crystallography.[6] Although we cannot exclude the possibility that the closed form of Ly49A observed in the Ly49A/H-2D^d structure is a crystal packing artifact, very recent results support the hypothesis that Ly49 receptors exist in both open and closed forms. Specifically, we have determined the crystal structure of another Ly49 receptor (Ly49L) in unbound form (E.L. Malchiodi, S. Cho & R.A.M., unpublished results). A notable feature of the Ly49 L dimer is that it adopts a closed conformation nearly identical with that of Ly49A in the Ly49A/H-2D^d structure. Thus, among the four available structures of Ly49 receptors in free or MHC-bound form (Ly49A/H-2D^d,[6] Ly49I,[8] Ly49C/H-2K^b,[7] Ly49L), two show the receptor as an open dimer (Ly49I, Ly49C/H-2K^b) and two as a closed dimer (Ly49A/H-2D^d, Ly49L). Together, these results suggest that Ly49s may exist on the NK cell surface in dynamic equilibrium between a closed form, which allows engagement of only one MHC molecule, and an open form, which permits bivalent binding. Which state predominates *in situ* may depend on a variety of still-undefined factors, which could include the conformation of the stalk region (see below), interactions with other proteins on the NK cell membrane, or local ionic conditions.

What might be the biological significance of the different conformational states observed for Ly49A, which likely characterize at least some other members of the Ly49 family? We propose a conformational switch mechanism for Ly49A in NK cell activation, by which variable dimerization of Ly49A allows differential binding of MHC, resulting in conformational control of NK cell function. Although speculative at this stage, this mechanism integrates the available structural and biological data on Ly49 receptors in a plausible way, and points the way to future investigation.

Recent studies of NK cell activation have demonstrated that the inhibitory Ly49A NK receptor binds to its H-2D^d ligand expressed on potential target cells (*trans* interaction), and is constitutively associated with H-2D^d on the NK cell itself (*cis* interaction).[29] Because *cis* and *trans* interactions involve the same binding sites, *cis* association restricts the number of Ly49A receptors available for binding to H-2D^d on target cells *in trans*. In contrast to *trans* interactions, *cis* interactions do not transmit negative signals to the NK cell, thereby lowering the threshold at which NK cell activation exceeds inhibition.[29] As a result, the sensitivity of the NK cell for generating a cytotoxic response is enhanced, allowing optimal discrimination between normal and MHC-deficient target cells.

We hypothesize that the closed state of Ly49A found in the crystal structure of the Ly49A/H-2D^d complex (Figure 5(a)) mediates *cis* interactions, whereas the predominantly open state of Ly49A observed in solution (Figure 5(c)) mediates *trans* interactions (Figure 8). To explain how Ly49A can bind MHC either *in cis* or *in trans*, we propose that the stalk regions linking the Ly49A dimer to the NK cell membrane are sufficiently flexible to permit very different orientations of the NKDs relative to the NK cell surface. Indeed, each Ly49A stalk region is exceptionally long (70 residues). Moreover, in the Ly49A dimer, the stalks are predicted to associate through a parallel coiled coil, in which coiled-coil regions are interspersed with several flexible portions that confer mobility to the ectodomain.[6] In the model (Figure 8), the Ly49A stalks adopt a back-folded, or bent, conformation to bind MHC *in cis* and an extended conformation to bind MHC *in trans*. We further propose that the bent conformation is associated with the closed Ly49A dimer, whereas the extended conformation is associated with the open dimer. The known inability of *cis* interactions to transmit inhibitory signals to the NK cell[29] may be

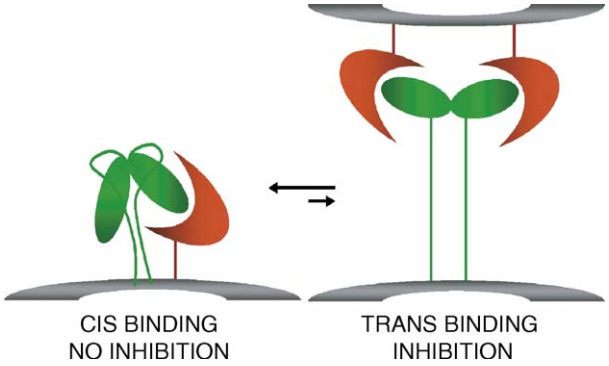

Figure 8. Model for *cis* and *trans* interactions of Ly49A with MHC. In the *cis* interaction (left), the "closed" Ly49A dimer (green) binds one MHC molecule (red) on the same NK cell. The stalk region of Ly49A bends back on itself to permit MHC engagement by the NKD. No inhibitory signal is transmitted to the NK cell. In the *trans* interaction (right), the "open" Ly49A dimer binds two MHC molecules on the target cell (top). To do so, the stalk region adopts an extended conformation. MHC cross-linking by the open Ly49A dimer stabilizes the *trans* interaction, resulting in transmission of inhibitory signals to the NK cell.

explained by the inability of the closed Ly49A dimer to bind a second MHC molecule and form a productive signaling complex. Conversely, engagement of two MHC molecules by the open Ly49A dimer stabilizes the *trans* interaction at the NK cell–target cell interface beyond the threshold required for NK signal transduction, inhibiting cytotoxic function. In this view, the Ly49A/H-2D^d and Ly49C/H-2D^d crystal structures (Figure 1) represent, respectively, non-productive and productive signaling complexes that were "captured" by different crystallization conditions or lattice contacts. It is notable that the proposed model bears certain similarities to the distinct conformational states adopted by integrins, in which bent and extended conformations regulate ligand binding and signal transmission.[30] However, validation of this, or any other, model for NK signal transduction will require coordinated structural and biological studies of Ly49–MHC interactions.

Materials and Methods

Protein expression, folding and purification

To label Ly49A with ^{2}H/^{13}C/^{15}N for NMR analysis, the NKD portion of the receptor (residues 127-262) was expressed in *Escherichia coli* BL21(DE3) cells as inclusion bodies in M9 minimal medium (^2H_2O solution, 13.0 g/l of KH_2PO_4, 10.0 g/l of K^2HPO_4, 9.0 g/l of Na^2HPO_4, 2.4 g/l of K_2SO_4, 10 μg/ml of thiamine, 1 mM $MgCl_2$, 100 μg/l of $CaCl_2$), supplemented with 2.5 g/l of [^{13}C]D-glucose and 1 g/l of [^{15}N]NH_4Cl, and enriched with ISOGRO ^{13}C-^{15}N-^{2}H-rich growth medium supplement (Isogro Isotec). The ^{2}H/^{13}C/^{15}N-enriched inclusion bodies were solubilized in 6 M guanidine and folded *in vitro* in 0.4 M arginine in the presence of 5.0 mM reduced glutathione and 0.5 mM oxidized glutathione, as described.[31] Folded protein was purified by anion-exchange and by size-exclusion chromatography, with sequential Poros HS-20 (POROS), Superdex 75 HR (Amersham Biosciences), and Mono S (Amersham Biosciences) columns.

For analytical ultracentrifugation experiments, unlabeled Ly49A NKD (wild-type and Asp193Gly mutant) was prepared as described.[31] Bacterial expression and assembly of H-2D^d containing synthetic P18-I10 peptide (RGPGRAFVTI) followed described procedures.[32]

NMR measurements

Final NMR samples were 280 μl in Shigemi thin-wall microcells, containing 0.2 mM Ly49A (dimer) in 93% H_2O, 7% ^2H_2O, either 25 mM or 320 mM NaCl, 25 mM phosphate, pH 7.0. Triple resonance NMR backbone assignment experiments and RDC measurements were carried out at 600 MHz ^{1}H frequency, using a Bruker DRX600 spectrometer equipped with a cryogenic probe head. Two ^{1}H-^{15}N-$^1H^N$ and ^{15}N-^{15}N-$^1H^N$ 3D NOESY spectra (Supplementary Data) were recorded at 800 MHz ^{1}H frequency, using a Bruker DRX800 spectrometer equipped with a cryogenic probe head. Backbone resonance assignments were made on the basis of TROSY versions of the 3D HNCO, 3D HNCA, 3D HNCOCA, 3D HN(COCA)CB, and 3D HN(CA)CB experiments, with ^{2}H decoupling during the periods where $^{13}C^\alpha$ or $^{13}C^\beta$ magnetization is transverse. Special attention was paid to restore the H_2O magnetization back to the +*z* axis before the start of each acquisition, thereby minimizing problems associated with solvent suppression and permitting somewhat faster repetition rates than would have been optimal if the water signal had become saturated. Typical measuring time for each of the backbone assignment experiments was one to three days. Total acquisition time for the pair of 3D NOESY spectra (250 ms mixing time) was three days.

Backbone ^{1}H-^{15}N RDC measurements were carried out at 320 mM NaCl, using 9 mg/ml Pf1 as a liquid crystalline alignment medium. Under these conditions, the Pf1 is no longer in the fully nematic state and shows paranematic behavior, with a field-dependent ^{2}H lock solvent splitting of 5.5 Hz and 4.0 Hz at 18.4 T and 14.1 T, respectively.[17] The high concentration of salt was found to be essential to prevent over-alignment and associated shortening of the ^{15}N transverse relaxation time. Comparison of the HNCO spectra recorded at low ionic strength (25 mM NaCl; 25 mM phosphate) with those where the concentration of NaCl was increased to 320 mM showed minimal changes in the resonance positions (rmsd $\Delta\delta(^1H^N)=0.05$ ppm, max$|\Delta\delta(^1H^N)|=0.13$ ppm; rmsd $\Delta\delta(^{15}N)=0.18$ ppm, max$|\Delta\delta(^{15}N)|=0.8$ ppm), indicating the absence of significant structural changes between the two ionic strength conditions. One-bond ^{1}H-^{15}N RDCs were collected from an interleaved pair of 3D TROSY-HNCO spectra, where either the TROSY or the anti-TROSY component was selected during ^{15}N evolution.[22,33] All spectral processing and data analysis was carried out using the software packages NMRPipe and PIPP.[34]

Structure calculations of the Ly49A dimer (chains A and B) were performed using the Xplor-NIH[35] and CNS[36] packages. A non-crystallographic symmetry (NCS) restraint term with a force constant of 10,000 kcal mol^{-1} Å^{-2} was defined between residues 140 and 258 of the two dimer chains. The coordinates of the A chain were kept fixed at the X-ray coordinates of chain D of the 1QO3

structure. A total of 104 unique H^N-N RDCs were input as a doubled set of 208 restraints acting on the two dimer chains. Inter-domain hydrogen bond geometries were optimized using the database backbone–backbone hydrogen bonding PMF with the explicitly listed H-bonded partners.[24] Standard repulsive-only, non-bonded interactions were used for the remainder of the inter-chain contacts. Although the two chains of the dimer are forced to be identical by standard application of the above-mentioned NCS term, such a procedure does not impose the C_2 symmetry of the dimer, identified by a single set of NMR resonances for residues at the interface. The C_2 symmetry of the dimer was enforced by, arbitrarily, splitting the definition of the group of residues that are related to one another and application of a second NCS restraint term (1000 kcal mol^{-1} $Å^{-2}$) acting between the following sets of C^{α} atoms: (A142–145; B 148–257) and (B 142–145; A 148–257). A slight modification of the code for the NCS restraint term (available upon request) was implemented to allow for the non-standard atom ordering associated with such residue pairing.

Analytical ultracentrifugation

Sedimentation velocity experiments were conducted at 20 °C in a Beckman Optima XL-I analytical ultracentrifuge at a rotor speed of 55,000 rpm (An50Ti rotor) with interference detection. Double-sector cells were loaded with 360–400 μl of proteins (Ly49A NKD alone, H-2D^d alone, or mixtures) that were first dialysed against phosphate-buffered saline (PBS), pH 7.4. Concentrations of mixtures at different molar ratios were used, with a constant concentration of Ly49A NKD (12 μM) added to increasing concentrations of H-2D^d (7 μM, 13 μM, 20 μM, 27 μM, 40 μM and 53 μM). Interference fringe displacement profiles were analyzed with the software SEDFIT‡, using a model for continuous sedimentation coefficient distribution $c(s)$ with deconvolution of diffusional effects.[37] The positions of meniscus and bottom, as well as time-invariant and radial noises, were fitted. Distributions were calculated with maximum entropy regularization at a predetermined confidence level of one standard deviation. In a further analysis, the differential sedimentation coefficient distribution $c(s)$ was integrated to determine weight-average sedimentation coefficients $s_w(c)$ as a function of H-2D^d concentration. The concentration dependence of $s_w(c)$ was analyzed by fitting the binding isotherms with two different models, corresponding to a 1:1 and 1:2 stoichiometry of H-2D^d to Ly49A dimer in the complex. The expression $s_w(c)$ was derived from mass action law and mass conservation equations. Two similar experiments were conducted independently and similar results were obtained. The s value in non-ideal conditions was corrected by a formula expressing the concentration-dependence of the sedimentation coefficient: $s_{corrected} = s_{apparent}/(1–kc)$, where c is the total protein concentration and k is the non-ideality coefficient for hard sphere repulsion (0.009 mg/ml).[38]

Similar sedimentation velocity experiments were conducted for Ly49A NKD bearing the Asp193Gly substitution. Mutant Ly49A (9 μM) was mixed with increasing concentrations of H-2D^d (5 μM, 10 μM, 15 μM, 20 μM, 25 μM, 30 μM, 35 μM and 40 μM). Results were analyzed as described for wild-type Ly49A NKD.

Sedimentation equilibrium ultracentrifugation experiments were done at 4 °C in an Optima XL-A instrument (Beckman Coulter) at rotor speeds of 15,000 rpm, 20,000 rpm and 25,000 rpm (An50Ti rotor). Absorbance data were acquired at 280 nm, 250 nm and 230 nm. Different concentrations of H-2D^d and Ly49A NKD (wild-type or D193G mutant) were mixed at a 2:1 molar ratio to total final concentrations of 0.07 mg/ml, 0.2 mg/ml, or 0.5 mg/ml. Protein samples were dialysed against PBS (pH 7.4), and 180 μl of protein mixture or free partner (0.2–0.3 mg/ml) were loaded into double-sector Epon centerpieces. Global non-linear regression was performed with the software SEDPHAT, using the equation for the radial concentration distribution of ideally sedimenting species in mechanical and chemical equilibrium. The data-fitting model of reversible heterogeneous interactions was determined from the mass action law combined with mass conservation equations,[39] assuming the interaction of one Ly49A dimer with two MHC molecules at two independent sites of binding. The theoretical extinction coefficient at 280 nm was calculated using the software SEDNTERP (provided by J. Philo) and was used to estimate from the sedimentation experiment the molar extinction coefficients at 250 and 230 nm in a global analysis. The bottom position of the solution column, as well as both radial and time-invariant noise, were determined by non-linear regression. A global and simultaneous fitting of all experimental data from the protein mixtures, at different rotor speeds and wavelengths, gave an estimation of the equilibrium dissociation constant K_D and χ^2.[39]

‡ www.analyticalultracentrifugation.com

Acknowledgements

This work was supported, in part, by the Intramural Research Program of the NIDDK, NIH (to A.B.), by the Intramural Antiviral Target Program of the Office of the Director, NIH (to A.B.), and by NIH grant AI47990 (to R.A.M.). We thank L. Deng for critical reading of the manuscript.

Supplementary Data

Supplementary data associated with this article can be found, in the online version, at doi:10.1016/j.jmb.2006.07.005

References

1. McQueen, K. L. & Parham, P. (2002). Variable receptors controlling activation and inhibition of NK cells. *Curr. Opin. Immunol.* **14**, 615–621.
2. Yokoyama, W. M. & Plougastel, B. F. M. (2003). Immune functions encoded by the natural killer gene complex. *Nature Rev. Immunol.* **3**, 304–316.
3. Desrosiers, M. P., Kielczewska, A., Loredo-Osti, J. C., Adam, S. G., Makrigiannis, A. P., Lemieux, S. *et al.* (2005). Epistasis between mouse Klra and major histocompatibility complex class I loci is associated with a new mechanism of natural killer cell-mediated innate resistance to cytomegalovirus infection. *Nature Genet.* **37**, 593–599.
4. Natarajan, K., Dimasi, N., Wang, J., Mariuzza, R. A. & Margulies, D. H. (2002). Structure and function of natural killer cell receptors: multiple molecular

solutions to self, nonself discrimination. *Annu. Rev. Immunol.* **20**, 853–885.
5. Anderson, S. K., Ortaldo, J. R. & McVicar, D. W. (2001). The ever-expanding Ly49 gene family: repertoire and signaling. *Immunol. Rev.* **181**, 79–89.
6. Tormo, J., Natarajan, K., Margulies, D. H. & Mariuzza, R. A. (1999). Crystal structure of a lectin-like natural killer cell receptor bound to its MHC class I ligand. *Nature*, **402**, 623–631.
7. Dam, J., Guan, R. J., Natarajan, K., Dimasi, N., Chlewicki, L. K., Kranz, D. M. *et al.* (2003). Variable MHC class I engagement by Ly49 natural killer cell receptors demonstrated by the crystal structure of Ly49C bound to H-2K^b. *Nature Immunol.* **4**, 1213–1222.
8. Dimasi, N., Sawicki, M. W., Reineck, L. A., Li, Y. L., Natarajan, K., Margulies, D. H. & Mariuzza, R. A. (2002). Crystal structure of the Ly49I natural killer cell receptor reveals variability in dimerization mode within the Ly49 family. *J. Mol. Biol.* **320**, 573–585.
9. Matsumoto, N., Mitsuki, M., Tajima, K., Yokoyama, W. M. & Yamamoto, K. (2001). The functional binding site for the C-type lectin-like natural killer cell receptor Ly49A spans three domains of its major histocompatibility complex class I ligand. *J. Expt. Med.* **193**, 147–157.
10. Wang, J., Whitman, M. C., Natarajan, K., Tormo, J., Mariuzza, R. A. & Margulies, D. H. (2002). Binding of the natural killer cell inhibitory receptor Ly49A to its major histocompatibility complex class I ligand: crucial contacts include both H-2Dd and b2-microglobulin. *J. Biol. Chem.* **277**, 1433–1442.
11. Wuthrich, K. (2003). NMR studies of structure and function of biological macromolecules (Nobel Lecture). *J. Biomol. NMR*, **27**, 13–39.
12. Folkers, P. J. M., Folmer, R. H. A., Konings, R. N. H. & Hilbers, C. W. (1993). Overcoming the ambiguity problem encountered in the analysis of nuclear Overhauser magnetic resonance spectra of symmetric dimer proteins. *J. Am. Chem. Soc.* **115**, 3798–3799.
13. Burgering, M. J. M., Boelens, R., Caffrey, M., Breg, J. N. & Kaptein, R. (1993). Observation of inter-subunit Overhauser effects in a dimeric protein. Application to the Arc repressor. *FEBS Letters*, **330**, 105–109.
14. Tjandra, N. & Bax, A. (1997). Direct measurement of distances and angles in biomolecules by NMR in a dilute liquid crystalline medium. *Science*, **278**, 1111–1114.
15. Prestegard, J. H., Al-Hashimi, H. M. & Tolman, J. R. (2000). NMR structures of biomolecules using field oriented media and residual dipolar couplings. *Quart. Rev. Biophys.* **33**, 371–424.
16. Hansen, M. R., Mueller, L. & Pardi, A. (1998). Tunable alignment of macromolecules by filamentous phage yields dipolar coupling interactions. *Nature Struct. Biol.* **5**, 1065–1074.
17. Zweckstetter, M. & Bax, A. (2001). Characterization of molecular alignment in aqueous suspensions of Pf1 bacteriophage. *J. Biomol. NMR*, **20**, 365–377.
18. Pervushin, K., Riek, R., Wider, G. & Wuthrich, K. (1997). Attenuated T-2 relaxation by mutual cancellation of dipole-dipole coupling and chemical shift anisotropy indicates an avenue to NMR structures of very large biological macromolecules in solution. *Proc. Natl Acad. Sci. USA*, **94**, 12366–12371.
19. Salzmann, M., Wider, G., Pervushin, K., Senn, H. & Wuthrich, K. (1999). TROSY-type triple-resonance experiments for sequential NMR assignments of large proteins. *J. Am. Chem. Soc.* **121**, 844–848.
20. Hitchens, T. K., Lukin, J. A., Zhan, Y. P., McCallum, S. A. & Rule, G. S. (2003). MONTE: An automated Monte Carlo based approach to nuclear magnetic resonance assignment of proteins. *J. Biomol. NMR*, **25**, 1–9.
21. Yang, D. W., Venters, R. A., Mueller, G. A., Choy, W. Y. & Kay, L. E. (1999). TROSY-based HNCO pulse sequences for the measurement of (HN)-H-1-N-15, N-15-(CO)-C-13, (HN)-H-1-(CO)-C-13, (CO)-C-13-C-13(alpha) and (HN)-H-1-C-13(alpha) dipolar couplings in N-15, C-13, H-2-labeled proteins. *J. Biomol. NMR*, **14**, 333–343.
22. Kontaxis, G., Clore, G. M. & Bax, A. (2000). Evaluation of cross-correlation effects and measurement of one-bond couplings in proteins with short transverse relaxation times. *J. Magn. Reson.* **143**, 184–196.
23. Losonczi, J. A., Andrec, M., Fischer, M. W. F. & Prestegard, J. H. (1999). Order matrix analysis of residual dipolar couplings using singular value decomposition. *J. Magn. Reson.* **138**, 334–342.
24. Grishaev, A. & Bax, A. (2004). An empirical backbone-backbone hydrogen-bonding potential in proteins and its applications to NMR structure refinement and validation. *J. Am. Chem. Soc.* **126**, 7281–7292.
25. Lovell, S. C., Davis, I. W., Adrendall, W. B., de Bakker, P. I. W., Word, J. M., Prisant, M. G. *et al.* (2003). Structure validation by Cα geometry: ϕ, ψ and Cβ deviation. *Proteins: Struct. Funct. Genet.* **50**, 437–450.
26. Dam, J. & Schuck, P. (2005). Sedimentation velocity analysis of heterogeneous protein-protein interactions: sedimentation coefficient distributions c(s) and asymptotic boundary profiles from Gilbert-Jenkins theory. *Biophys. J.* **89**, 651–666.
27. Dam, J. & Schuck, P. (2004). Calculating sedimentation coefficient distributions by direct modeling of sedimentation velocity concentration profiles. *Methods Enzymol.* **384**, 185–212.
28. de la Torre, J. G., Huertas, M. L. & Carrasco, B. (2000). Calculation of hydrodynamic properties of globular proteins from their atomic-level structure. *Biophys. J.* **78**, 719–730.
29. Doucey, M. A., Scarpellino, L., Zimmer, J., Guillaume, P., Luescher, I. F., Bron, C. & Held, W. (2004). Cis association of Ly49A with MHC class I restricts natural killer cell inhibition. *Nature Immunol.* **5**, 328–336.
30. Shimaoka, M. & Springer, T. A. (2003). Therapeutic antagonists and conformational regulation of integrin function. *Nature Rev. Drug Discov.* **2**, 703–716.
31. Natarajan, K., Boyd, L. F., Schuck, P., Yokoyama, W. M., Eilat, D. & Margulies, D. H. (1999). Interaction of the NK cell inhibitory receptor Ly49A with H-2Dd: Identification of a site distinct from the TCR site. *Immunity*, **11**, 591–601.
32. Li, H. M., Natarajan, K., Malchiodi, E. L., Margulies, D. H. & Mariuzza, R. A. (1998). Three-dimensional structure of H-2D^d complexed with an immunodominant peptide from human immunodeficiency virus envelope glycoprotein 120. *J. Mol. Biol.* **283**, 179–191.
33. Yang, D. W., Venters, R. A., Mueller, G. A., Choy, W. Y. & Kay, L. E. (1999). TROSY-based HNCO pulse sequences for the measurement of (HN)-H- 1-N-15, N-15-(CO)-C-13, (HN)-H-1-(CO)-C-13, (CO)-C-13-C-13(alpha) and (HN)-H-1-C-13(alpha) dipolar couplings in N-15, C-13, H-2-labeled proteins. *J. Biomol. NMR*, **14**, 333–343.
34. Delaglio, F., Grzesiek, S., Vuister, G. W., Zhu, G., Pfeifer, J. & Bax, A. (1995). NMRpipe: a multidimensional spectral processing system based on Unix pipes. *J. Biomol. NMR*, **6**, 277–293.
35. Schwieters, C. D., Kuszewski, J. J., Tjandra, N. & Clore, G. M. (2003). The Xplor-NIH NMR molecular structure determination package. *J. Magn. Reson.* **160**, 65–73.

36. Brunger, A. T., Adams, P. D., Clore, G. M., DeLano, W. L., Gros, P., Grosse-Kunstleve, R. W. *et al.* (1998). Crystallography & NMR system: a new software suite for macromolecular structure determination. *Acta Crystallog. sect. D*, **54**, 905–921.
37. Schuck, P., Perugini, M. A., Gonzales, N. R., Howlett, G. J. & Schubert, D. (2002). Size-distribution analysis of proteins by analytical ultracentrifugation: strategies and application to model systems. *Biophys. J.* **82**, 1096–1111.
38. Harding, S. E. & Johnson, P. (1985). The concentration-dependence of macromolecular parameters. *Biochem. J.* **231**, 543–547.
39. Vistica, J., Dam, J., Balbo, A., Yikilmaz, E., Mariuzza, R. A., Rouault, T. A. & Schuck, P. (2004). Sedimentation equilibrium analysis of protein interactions with global implicit mass conservation constraints and systematic noise decomposition. *Anal. Biochem.* **326**, 234–256.

Edited by M. F. Summers

(Received 2 May 2006; received in revised form 19 June 2006; accepted 3 July 2006)
Available online 8 August 2006